Scale of experiment and rock physics trends

JACK DVORKIN, Stanford University and AMOS NUR, Ingrain

Because rock is heterogeneous at all scales, it is often invalid to assign a single porosity, permeability, resistivity, or velocity to a volume in the subsurface. Well data demonstrate that these properties can vary appreciably between two points just a foot apart. The same happens at the pore scale. Consider, for example, a CT scan of a 1.3-mm Berea sandstone cube (Figure 1). The porosity of this sample, as calculated by counting the blue (pore space) pixels, is 0.164.

Let us next evenly subdivide this cube into 8 (2^3) subcubes. The porosity of these subsamples can be as high as 0.189 and as low as 0.140 (Figure 2, left).

A more dramatic example of the spatial nonstationarity of porosity is shown by a 3.138 mm oil-sand sample (Figure 3). The porosity of this sample is 0.258. The maximum porosity among the eight subsamples (obtained in the same way as for the Berea sandstone) is 0.361, while the minimum porosity is 0.206 (Figure 2, right). This strong spread of the subsampled porosity is due to the high heterogeneity of the original cube: in addition to small and medium-size pores, it contains a relatively wide fracture.

To estimate the resulting spatial nonstationarity of the elastic-wave velocity, we assume that in Berea sandstone, which is clean and consolidated, V_P is related to porosity by the Raymer et al. (1980) equation, $V_P = (1-\phi)^2 V_{PS} + \phi V_{PF}$, where V_{PS} is the velocity in the solid phase of the rock, V_{PF} is the velocity in the fluid, and ϕ is porosity. We also assume that the matrix is quartz (V_{PS} = 6.04 km/s) and the sample is dry (V_{PF} = 0).

For the oil sand, we assume that its velocity is related to porosity by the soft-sand model (Dvorkin and Nur, 1996), which is appropriate for this unconsolidated sample. As in the Berea case, we use the pure-quartz mineralogy and calculate V_P for the dry sample, neglecting the effect of the oil.

The resulting velocity-porosity plots show discernable spatial spread of V_P, from 4.00 to 4.50 km/s in Berea and from 1.59 to 2.17 km/s in the oil sand (Figure 4). Because these sets of velocities are drawn from within small volumes of rock (essentially, from a point in space), we speculate that it may be invalid to attribute a single porosity and/or a velocity value to a volume in a rock sample or in a geobody.

Data points and trends: Elasticity

To deal with the spatial nonstationarity of rock properties, we need to find a quantity alternative to a velocity-porosity data point, a quantity that is stationary in space. We hypothesize that a trend between two or more rock properties can be this quantity.

To explore this hypothesis, consider first a cubic volume of rock that includes 125 equal-cube elements, each with fixed porosity (ϕ) and clay content (C). Both C and ϕ randomly vary among the elements in the respective intervals of zero to 0.1 and 0.1 to 0.3 (Figure 5). Let us assume that the velocity in each of the 125 elements is related to ϕ and C

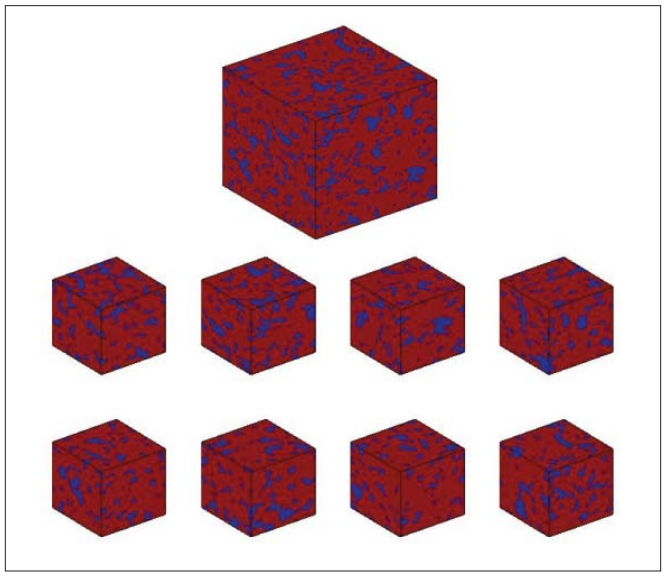

Figure 1. *Top: The original 3D Berea cube. The resolution is 8.6 μm per pixel. The size is 150 × 150 × 150 pixels (1.3 × 1.3 × 1.3 mm). Middle and bottom: eight subcubes. The size of each subcube is 75 × 75 × 75 pixels (0.65 × 0. 65 × 0. 65 mm). The first subcube has the highest porosity (0.189) while the third one has the lowest porosity (0.140).*

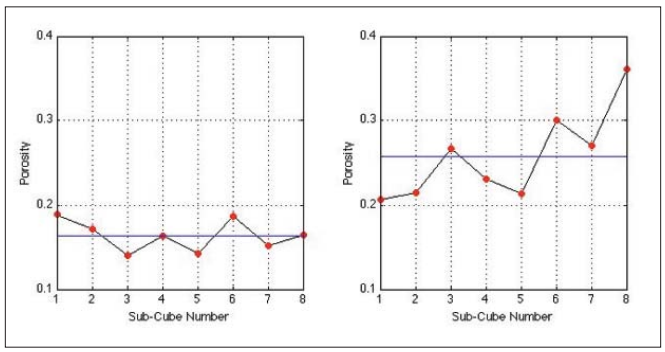

Figure 2. *Porosity (red) in the eight subsamples of the original cube. The horizontal line is the porosity of the original cube. Left: Berea sandstone. Right: oil sand.*

by the Raymer equations for both V_P (same as quoted in the previous section) and V_S, as is appropriate for mature fast rock (Dvorkin, 2008):

$$V_P = (1-\phi)^2 V_{PS} + \phi V_{PF}, \qquad (1)$$

$$V_S = (1-\phi)^2 V_{SS} \sqrt{\frac{(1-\phi)\rho_S}{(1-\phi)\rho_S + \phi\rho_F}},$$

where V_{PS} and V_{SS} are the P- and S-wave velocities in the mineral matrix, respectively. V_{PF} is the velocity in the pore fluid, and ρ_S and ρ_F are the densities of the mineral matrix and pore fluid, respectively. The pore fluid in this example is water with bulk modulus 2.6 GPa, density 1 g/cc, and veloc-

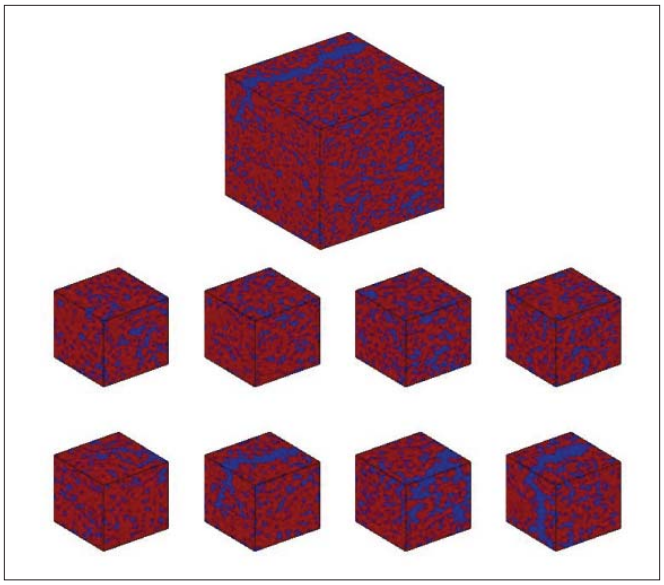

Figure 3. *Top: the original 3D oil sand cube. The resolution is 20.9 μm per pixel. The size is 150 × 150 × 150 pixels (3.138 × 3.138 × 3.138 mm). Middle and bottom: eight subcubes. The size of each subcube is 75 × 75 × 75 pixels (1.569 × 1.569 × 1.569 mm). The first subcube has the lowest porosity (0.206), while the last one has the highest porosity (0.361).*

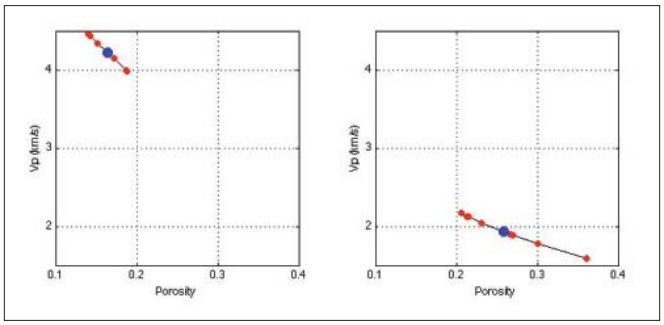

Figure 4. *Velocity versus porosity for the eight subcubes (red) and for the original cube (blue), theoretically obtained from porosity, as described in the text. Left: Berea sandstone. Right: oil sand.*

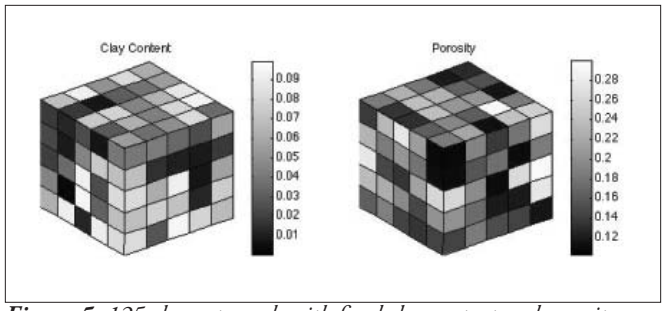

Figure 5. *125 elements, each with fixed clay content and porosity, forming a larger volume. Clay content (left) and porosity (right).*

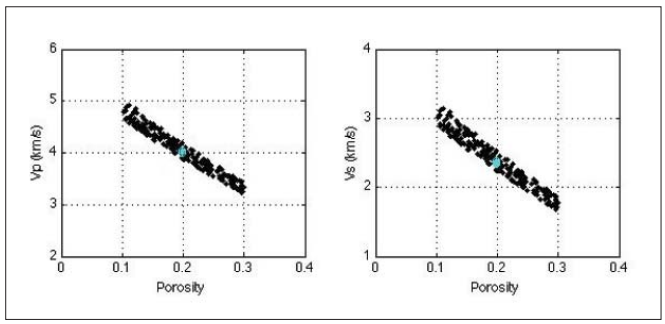

Figure 6. *Velocity versus porosity for the 125 elements shown in Figure 5, assuming that the velocity in each element is described by Equation 1. The P-wave velocity is on the left, while the S-wave velocity is on the right. The cyan symbols are the upper and lower HSB.*

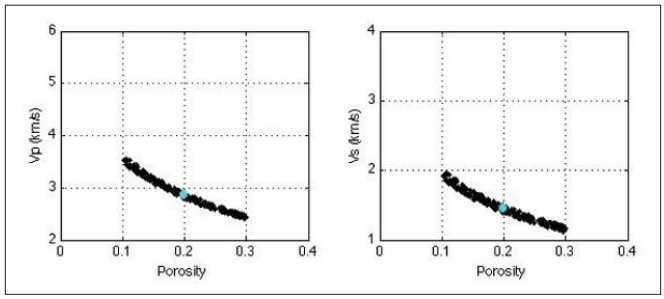

Figure 7. *Same as Figure 6, but for the soft-sand model.*

ity 1.613 km/s.

The velocity thus obtained is plotted versus porosity in Figure 6. As expected, it forms a tight velocity-porosity trend with a small vertical spread, due to variable clay content, at a fixed porosity.

To bracket the effective elastic properties of the larger cube formed by these 125 elements, we assume that the larger cube is elastically isotropic and then apply the upper and lower Hashin-Shtrikman (1963) elastic bounds (HSB), with each element treated as a constituent of the elastic composite with a constant volume fraction 1/125 = 0.008. The resulting upper and lower bounds for V_P and V_S are plotted in Figure 6 versus the average porosity ϕ_{Eff}, which is the arithmetic average of the porosity of each element: $\phi_{Eff} = \langle \phi \rangle$.

First and foremost, we observe that the HSB for both V_P and V_S are very close to each other and practically indistinguishable. In addition, they fall directly on the velocity-porosity trend formed by the 125 elements. This means that the effective velocity, which must be located between these tight bounds, obeys the same velocity-porosity transform as the 125 elements of the volume under examination. An important conclusion is that although the porosity and velocity vary within wide ranges inside the large cube, the velocity-porosity trend does not. This trend exhibits spatial stationarity. This conclusion remains valid if instead of Equation 1 we use a different model, namely the soft-sand model of Dvorkin and Nur (1996), appropriate for soft, slow sediment (Figure 7).

Instead of using velocity-porosity equations to create a heterogeneous volume, we can adopt a laboratory data set obtained on samples of a similar type within a range of porosity. Then we will stage a thought experiment and make a single heterogeneous sample from this data set, by assuming, e.g., that the subsamples enter this larger sample in equal volumetric proportions. An example of this approach is shown in Figure 8, where we use Han's (1986) dry-rock velocity data in a wide range of porosity, with clay content ranging from zero to 0.15. These data form tight velocity-porosity trends for both V_P and V_S. The HSB calculated in the same fashion

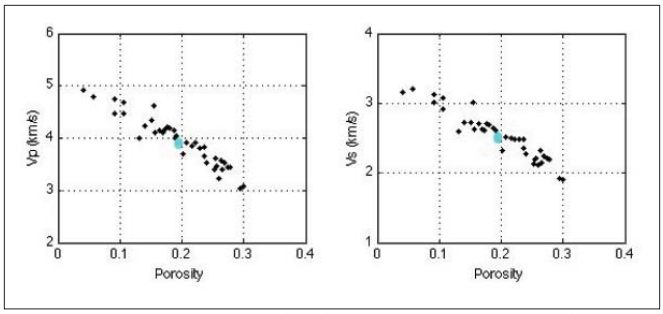

Figure 8. *Same as Figure 6, but for Han's (1986) data, with clay content between zero and 0.15.*

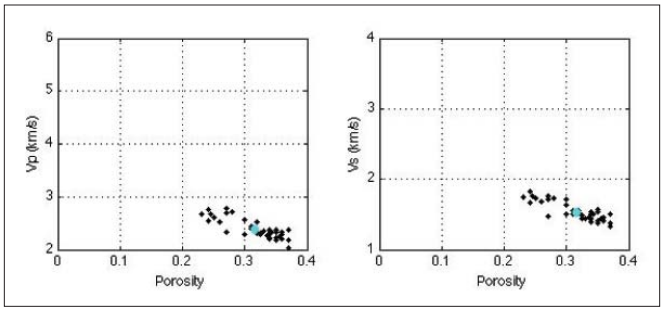

Figure 9. *Same as Figure 6, but for Blangy's (1992) data.*

as in the earlier examples are very close to each other and fall precisely on these trends.

A similar real-data example, but for high-porosity soft sand obtained by Blangy (1992) on room-dry samples from the Troll Field is shown in Figure 9. These results prove that although rock properties may spatially vary inside a volume and, therefore, be scale-dependent, the trends between them (under the conditions used in these examples) persist at varying scales.

Two important points have to be kept in mind regarding the above treatment of elastic heterogeneity. First, the approach used is essentially a low-frequency approach. This means that the wavelength is larger than each of the elements of the composite and also is large enough to perceive the whole composite as a body with single values of velocity, porosity, and clay content. At higher frequencies (smaller wavelength) "fast tracking" of elastic waves through the sample may occur if some of the elements form a fast path.

Second, the parameters in the relation between velocity and porosity and clay content may themselves be uncertain, which would increase the spread. Treating this type of uncertainty is beyond the objectives of this paper, although it is within the framework of this approach: generally, the trends have to be expressed as probability distributions around the main trend, not just as the spread in porosity and clay content.

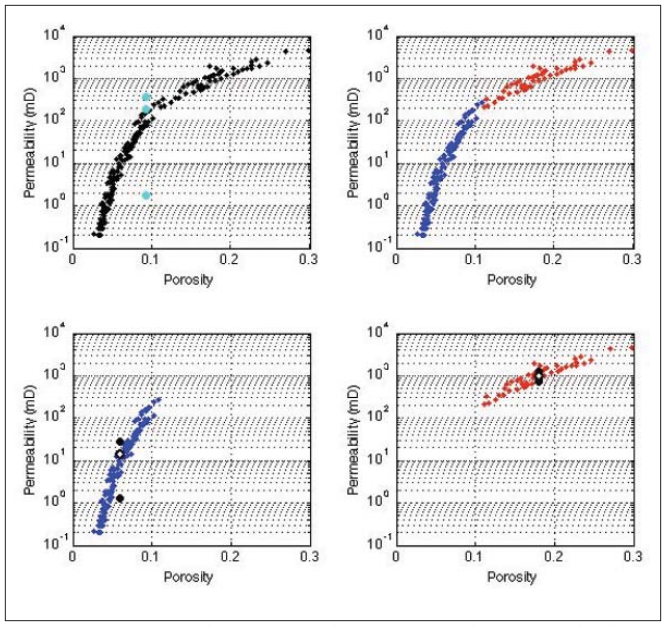

Figure 10. *Fontainebleau permeability-porosity data. Top left: the entire data set (165 samples) with the upper and lower permeability bounds and their arithmetic average shown as cyan symbols. Top right: the data divided into two subsets, below porosity 0.1 (119 samples, blue) and above porosity 0.1 (46 samples, red). Bottom left: the subset with porosity below 0.1, with the upper and lower bounds (filled black symbols) and their arithmetic average (the open black symbol). Bottom right: the subset with porosity above 0.1, with the upper and lower bounds (filled black symbols) and their arithmetic average (the open black symbol). The bounds and their averages are plotted versus the respective arithmetic average of porosity for each data set displayed.*

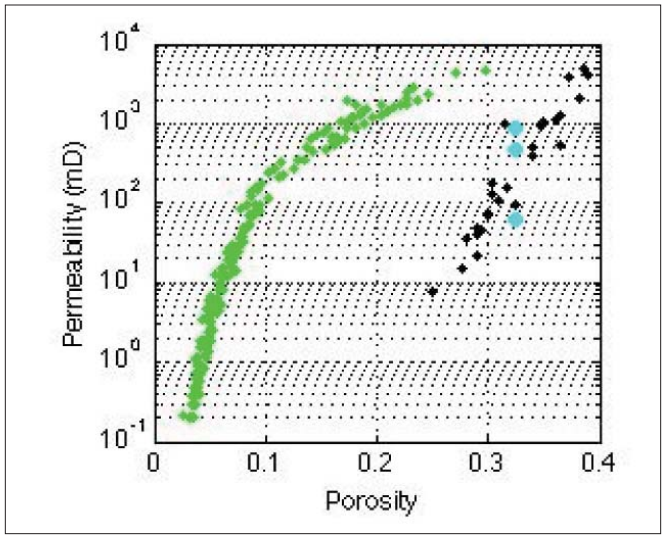

Figure 11. *Troll permeability-porosity data (filled black symbols). The cyan symbols are the lower and upper permeability bounds and their arithmetic average plotted versus the arithmetically averaged porosity. The Fontainebleau data are shown for comparison as green symbols.*

Data points and trends: Permeability

Permeability is arguably the only property that cannot be directly inferred from well data. Let us concentrate on this parameter, which is crucial to the petroleum engineer.

Consider first the classical Fontainebleau sandstone permeability-porosity (k-ϕ) data (Bourbie and Zinszner, 1985), which are used in many permeability-related analyses. The porosity range in this data set is from 0.03 to 0.30, with the corresponding permeability variation between 0.2 and 4,772.0 mD (Figure 10). The average porosity among these samples, calculated as $\langle\phi\rangle$, is 0.093.

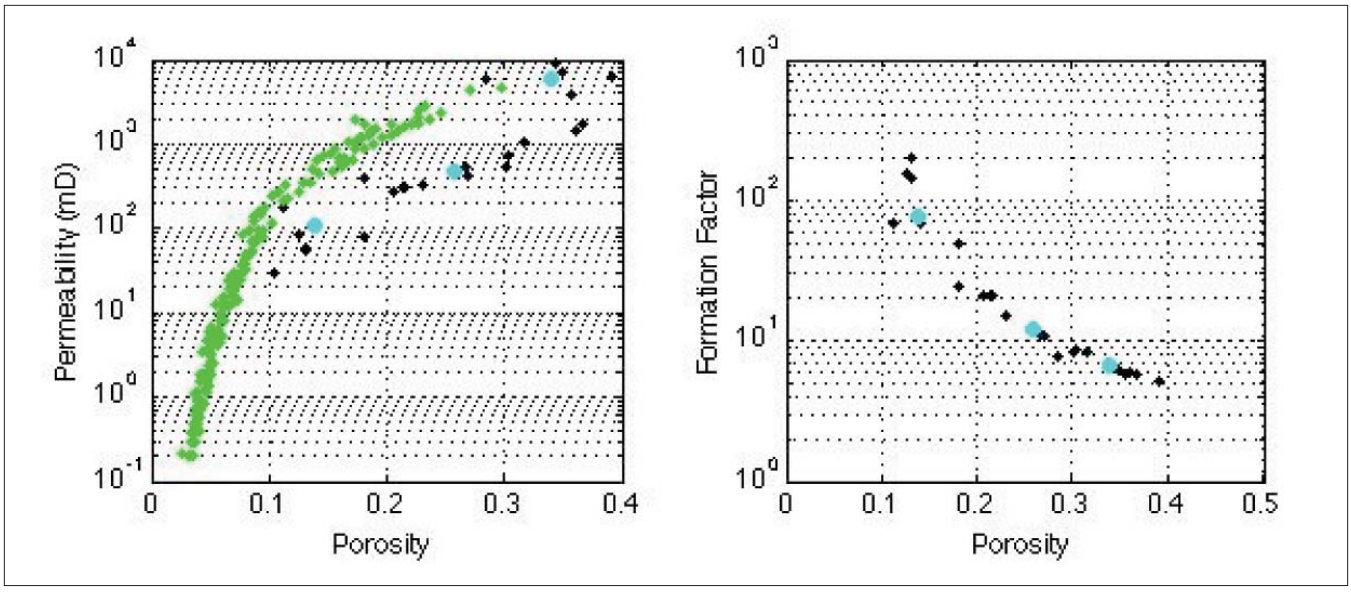

Figure 12. *Berea sandstone and two oil-sand samples. Permeability (left) and formation factor (right) versus porosity. Filled black symbols are for the eight subcubes for each of the three digital samples (24 subsamples altogether). Cyan symbols are for the original larger cubes for each of the three digital samples. The green symbols in the permeability-porosity plot are for the Fontainebleau data set, plotted here for comparison.*

For a hypothetical large volume comprised of these fixed-porosity elements, we calculate the upper bound as the arithmetic average of the elemental permeability values (k) and the lower bound as their harmonic average $(k^{-1})^{-1}$. This lower bound is 1.77 mD while the upper one is 371.48 mD. These bounds fall far apart from each other when plotted versus the average porosity (ϕ), yet they are tighter than the whole range of permeability (0.2 to 4,772.0 mD). Their arithmetic average, 186.63 mD, falls right on the permeability-porosity trend formed by the individual samples (Figure 10).

To constrain the range of applicability of our reasoning, let us subdivide this dataset into two parts, one for porosity below 0.1 and the other above this value. The lower and upper permeability bounds are still far apart from each other for the former case, although their arithmetic average falls right on the k-ϕ trend for this subset. The situation becomes much more interesting for the latter data set. Here the lower and upper k bounds are very tight and, once again, lie on the corresponding k-ϕ trend (Figure 10).

This means that our conclusion for elastic data holds for permeability data if the latter (k) varies within a relatively constrained interval (about 1.5 orders of magnitude): a k-ϕ trend exhibited by elements persists for the composite of these elements.

Our next permeability example for high-porosity samples from the Troll Field (courtesy Norsk Hydro), similar to the samples used in Figure 9, is displayed in Figure 11. Here, the porosity varies between 0.25 and 0.39 with the permeability varying between 8 and 5,000 mD.

This trend is very different from the Fontainebleau trend: the permeability rapidly decays with decreasing porosity, mainly because the reduction of the latter is due to deteriorating grain sorting and decreasing average grain size. Still, the upper and lower bounds (62 and 883 mD, respectively), although far apart from each other, straddle the elemental trend. Their arithmetic average (473 mD), if plotted versus the average porosity (0.325), falls upon this elemental trend.

From a whole to parts: Digital rock physics

We have proved so far that by putting together many different elements with two spatially nonstationary properties that form a trend, we create a composite whose same two properties obey this trend (very accurately for the elastic properties and with certain stipulations for permeability). How do we address the opposite situation, where we desire to break a composite into many parts?

Such experiments would be very difficult to stage in the physical laboratory, simply because the parts are smaller than the whole, while most experimental setups require similarly-sized samples for obtaining internally consistent data sets. This is where digital rock physics takes over from traditional experimental rock physics. Within the framework of the former, we can accurately image essentially any irregularly shaped rock fragment, select any desired subsamples of this fragment, and then stage an accurate computational simulation of an experiment on each subsample as well as on the original volume. Such volumes and their subsamples are displayed in Figures 1 and 3.

Let us now simulate a single-phase fluid flow in these volumes and their eight subcubes, as well as in a third digital sample of oil sand, whose porosity is larger than that of the oil sand displayed in Figure 3. The computational engine used here is the lattice-Boltzmann method (e.g., Keehm et al., 2001). The result of this digital experiment is displayed in Figure 12. The three original samples form a distinctive permeability-porosity trend, and their eight subsamples (24 subsamples altogether for these three samples) obey approximately the same trend. This means that by breaking a whole into parts and conducting experiments on these parts, we ob-

tain a spatially stationary trend from the individual properties (porosity and permeability), which are not spatially stationary.

A digital experiment result for the electrical formation factors of the same three samples is also shown in Figure 12. Once again, we observe the stationarity of a trend between two spatially nonstationary properties.

Conclusion

The heterogeneity of natural rock that persists at many scales calls into question the practical utility of data obtained on a given sample, which is, in effect, a point in the space occupied by the rock. How can we use such data in the context of remote sensing, which samples different and differently-sized volumes within a formation?

The examples presented here indicate that under certain, possibly limited, circumstances, trends formed by pairs of data points obtained on an internally heterogeneous dataset form a trend that is valid over a range of scales. Such a trend is stationary with respect to position and scale, and so can be applied to a remotely sensed quantity (e.g., porosity) to arrive at another desired property (e.g., permeability) at the scale of practical measurement.

This property of a trend is akin to ergodicity in theoretical physics and statistics, also called "statistical stationarity" and usually described in terms of objective properties of an ensemble of diverse objects. The ergodicity of natural-rock data, as discussed here, means that we may hope "to see a rock in a grain of sand" (Kameda and Dvorkin, 2004). Digital rock physics is the contemporary tool to explore this ergodicity and chart its applicability to remote sensing and other practical problems.

Suggested reading. *Integrated Seismic Lithologic Interpretation: The Petrophysical Basis* by Blangy (PhD dissertation, Stanford University, 1992). "Hydraulic and acoustic properties as a function of porosity in Fontainebleau sandstone" by Bourbie and Zinszner (*Journal of Geophysical Research*, 1985). "Yet another V_S equation" by Dvorkin (GEOPHYSICS, 2008). "Elasticity of high-porosity sandstones: Theory for two North Sea datasets" by Dvorkin and Nur (GEOPHYSICS,1996). "Effects of porosity and clay content on acoustic properties of sandstones and unconsolidated sediments" by Han (Stanford University, 1986). "A variational approach to the elastic behavior of multiphase materials" by Hashin and Shtrikman (*Journal of Mechanics and Physics of Solids,* 1963). "To see a rock in a grain of sand" by Kameda and Dvorkin (*TLE,* 2004). "Computational rock physics at the pore scale: Transport properties and diagenesis in realistic pore geometries" by Keehm et al. (*TLE*, 2001). "An improved sonic transit time-to-porosity transform" by Raymer et al. (*Transactions of the Society of Professional Well Log Analysts*, 1980). TLE

Corresponding author: dvorkin@stanford.edu